DMD Fast Forward. Published on November 21, 2011 as doi: 10.1124/dmd.111.042739

Title page

Stereospecific Metabolism of Itraconazole by CYP3A4: Dioxolane Ring Scission of Azole Antifungals

Chi-Chi Peng, Wei Shi, Justin D. Lutz, Kent L. Kunze, Jun O. Liu, Wendel L. Nelson, Nina Isoherranen

Department of Pharmaceutics (CP, NI, JDL) and Department of Medicinal Chemistry (KLK and WLN), University of Washington, Seattle, Washington; Department of Pharmacology and Molecular Sciences, Johns Hopkins School of Medicine, Baltimore, Maryland (WS, JOL)

Running title page:

Running title: Dioxolane ring scission of itraconazole by CYP3A4

Author for correspondence: Nina Isoherranen, PhD Department of Pharmaceutics, University of Washington Box 357610, Seattle WA

Fax: 206-543-3204, Tel: 206-543-2517

e-mail: ni2@u.washington.edu

number of text pages: 17

number of tables: 2

number of figures: 8

number of references: 18

number of words in abstract: 246

number of words in introduction: 527

number of words in discussion: 1069

List of abbreviations: ITZ-itraconazole; KPi-Potassium Phosphate; HLM-Human liver microsomes; MDZ-midazolam; DDI-drug-drug interactions; SPR-surface plasmon resonance

DMD Fast Forward. Published on November 21, 2011 as DOI: 10.1124/dmd.111.042739
This article has not been copyedited and formatted. The final version may differ from this version.

ABSTRACT

Itraconazole (ITZ) is a mixture of four *cis*-stereoisomers which inhibit CYP3A4 potently and coordinate CYP3A4 heme via the triazole nitrogen. However (2R,4S,2'R)-ITZ and (2R,4S,2'S)-ITZ also undergo stereoselective sequential metabolism by CYP3A4 at a site distant from the triazole ring to 3'-OH-ITZ, keto-ITZ and N-desalkyl-ITZ. This stereoselective metabolism demonstrates specific interactions of ITZ within the CYP3A4 active site. To further investigate this process, the binding and metabolism of the four *trans*-ITZ stereoisomers by CYP3A4 was characterized. All four *trans*-ITZ stereoisomers were tight binding inhibitors of CYP3A4 mediated midazolam hydroxylation (IC_{50} 16-26 nM) and each gave a type II spectrum upon binding to CYP3A4. However, instead of formation of 3'-OH-ITZ they were oxidized at the dioxolane ring leading to ring scission and formation of two new metabolites of ITZ. These two metabolites were also formed from the four *cis*-ITZ stereoisomers although not as efficiently. The catalytic rates of dioxolane ring scission were similar to the dissociation rate of ITZ stereoisomers from CYP3A4, suggesting that the heme iron is reduced while the triazole moiety coordinates to it and no dissociation of ITZ is necessary prior to catalysis. The triazole containing metabolite (1-(2,4-dichlorophenyl)-2-(1H-1,2,4-triazol-1-yl)ethanone) also inhibited CYP3A4 (IC_{50}>15 μM) and showed type II binding with CYP3A4. The dioxolane ring scission appears to be clinically significant as this metabolite was detected in urine samples from subjects that had been administered the mixture of *cis*-ITZ isomers. These data suggest that the dioxolane ring scission is a metabolic pathway for drugs that contain this moiety.

Introduction

Itraconazole (ITZ) is a broad-spectrum antifungal agent that was designed to inhibit the fungal P450 enzyme lanosterol demethylase by coordinating the heme of the P450 via the triazole nitrogen (Vanden Bossche et al., 1989; Haria et al., 1996). Itraconazole is also a potent inhibitor of human P450 enzymes, specifically CYP3A4 resulting in potent drug-drug interactions with CYP3A4 substrates (Isoherranen et al., 2004; Templeton et al., 2008). In addition to CYP3A4 inhibition, the clinical use of ITZ is limited by its rare hepatotoxicity (Wang et al., 2010). Although ITZ contains three chiral centers (at C-2 and C-4 in the dioxolane ring and at C-2' on the sec-butyl side chain), resulting in a total of eight possible ITZ stereoisomers (Scheme 1), a mixture of 4 of them with *cis* configuration in the dioxolane ring is marketed. Representative *cis*- and *trans*-ITZ are shown in Scheme 1.

All four *cis*-ITZ stereoisomers are high affinity ligands of CYP3A4 and produce type II binding spectra with CYP3A4 indicating that the triazole nitrogen coordinates the heme iron (Kunze et al., 2006). However, two of the four marketed ITZ stereoisomers, (2R,4S,2'R)-ITZ and (2R,4S,2'S)-ITZ, also undergo metabolism by CYP3A4 to form 3'-OH-, keto- and N-desalkyl-ITZ (Scheme 1). The formation of 3'-OH-, keto- and N-desalkyl-ITZ results from oxidation of ITZ at the opposite end of the molecule from the triazole ring that coordinates to the heme (Kunze et al., 2006). Hence metabolism to the 3'-OH-ITZ requires either reorientation of ITZ within the CYP3A4 active site or dissociation of the type II complex and rebinding of ITZ in the catalytically productive orientation. The latter process was previously shown to be likely for (2R,4S,2'R)-ITZ based on surface plasmon resonance (SPR) experiments (Pearson et al., 2006). However, the reasons for the observed stereoselectivity in ITZ metabolism have not been elucidated.

Recently all eight stereoisomers of ITZ were reported with evaluation of their antifungal and antiangiogenic activity (Shi et al., 2010). In cell culture models, the *trans*-ITZ stereoisomers (2R,4R,2'R)-, (2R,4R,2'S)-, (2S,4S,2'R)- and (2S,4S,2'S)-ITZ were less potent than *cis*-ITZ

stereoisomers in antiangiogenesis activity, but two of the *trans*-ITZs (2S,4S pair) were as potent as the *cis*-diastereomers in their antifungal activity (Shi et al., 2010). Whether these *trans*-ITZs inhibit and/or are metabolized by CYP3A4 is unknown. Based on the observed stereoselectivity in *cis*-ITZ metabolism by CYP3A4 it was hypothesized that the metabolism of *trans*-ITZ stereoisomers would be stereoselective, and that all four stereoisomers would inhibit CYP3A4 and coordinate the heme iron via the triazole nitrogen. The aims of this study were to determine whether 1) *trans*-ITZ stereoisomers are potent, stereoselective inhibitors of CYP3A4, 2) *trans*-ITZ stereoisomers bind to CYP3A4 with similar affinity as *cis*-ITZs in type II fashion, and 3) *trans*-ITZs are metabolized by CYP3A4 at similar sites as the *cis*-ITZ isomers. A novel metabolite resulting from dioxolane ring scission was identified from both *cis*- and *trans*-ITZs, and the kinetics of the formation of this metabolite was characterized. The inhibition of CYP3A4 by the 1-(2,4-dichlorophenyl)-2-(1H-1,2,4-triazol-1-yl)ethanone metabolite (M2) was also examined and the formation of this metabolite *in vivo* in humans was established. This metabolic pathway may be important for other antifungal drugs that have the dioxolane ring in their structures such as ketoconazole.

DMD Fast Forward. Published on November 21, 2011 as DOI: 10.1124/dmd.111.042739
This article has not been copyedited and formatted. The final version may differ from this version.

Materials and Methods

Chemicals and Reagents: *trans*-Itraconazole stereoisomers were synthesized as previously published (Shi et al., 2010), *cis*-ITZ stereoisomers were gifts from Sepracor Inc. (Marlborough, MA). 3'-OH-ITZ was purchased from Research Diagnostics Inc. (Flanders, NJ), keto-ITZ was provided by Janssen Pharmaceutica N. V. (Beerse, Belgium) and N-desalkyl-ITZ was prepared as previously reported (Kunze et al., 2006). Midazolam, 1'-hydroxymidazolam (OH-MDZ) and 1'-hydroxymidazolam-d_4 were purchased from Cerilliant (Round Rock, Texas). 1-(2,4-dichlorophenyl)-2-(1H-1,2,4-triazol-1-yl)ethanone was purchased from ChemBridge Screening Library (San Diego, CA,). Ammonium chloride was obtained from Mallinckrodt Baker (Phillipsburg, NJ), and HPLC-grade methanol, acetonitrile (ACN) and ethyl acetate were obtained from Fisher Scientific (Fairlawn, NJ). NADPH was from Sigma-Aldrich. CYP3A4 supersomes^{TM} coexpressed with cytochrome P450 reductase and cytochrome b5 were purchased from BD Biosciences (Woburn, MO). Pooled HLMs were prepared from three livers (all CYP3A5 *3/*3 genotype) obtained from the human liver bank of the University of Washington, using equal microsomal protein amounts from each liver to make the pooled stock HLM. The CYP3A4 NF14 construct was expressed and purified from *Eschericia coli* as previously described (Gillam et al., 1993). The CYP3A4 concentration was determined by CO difference spectrum using the ε 450 of 91 mM^{-1} cm^{-1}(Omura and Sato, 1964). CYP3A4 was stored at -80^{o}C in 20 % glycerol 80% 100 mM potassium phosphate (KPi) buffer (pH 7.4).

IC_{50} determination of *trans*-itraconazole stereoisomers towards CYP3A4: Pooled human liver microsomes (0.025 mg/mL, CYP3A5 *3/*3) and midazolam (1 μM, MDZ) were incubated with varying concentrations of *trans*-ITZ isomers (5 nM-1000 nM) in 0.5 mL KPi buffer to determine IC_{50}. The 1 μM concentration of MDZ which is $<<K_m$ for MDZ (4 μM) was used to assure the IC_{50} value determined is not dependent on the mechanism (competitive or noncompetitive) of inhibition, or elevated due to

competition of CYP3A4 between the substrate and inhibitor. The reaction mixtures were preincubated for 5 minutes at 37 °C and initiated by adding NADPH (final concentration 1 mM). After 2 minutes, the reaction was stopped by adding 1 mL of ethyl acetate. Internal standard (20 µL of 0.1 µg/mL 1'-OH-MDZ- d_4) was added to each sample. The organic phase was evaporated to dryness under nitrogen stream, reconstituted in 100 µL of 1:1 methanol/water (v/v), transferred to LC/MS vials and analyzed as previously described (Isoherranen et al., 2004) using a Waters Micromass Platform LCZ: Quadrupole Mass Spectrometer (Waters, Milford, MA) operated on the positive ion electrospray mode, monitoring ions m/z 342.2 for 1'-OH-MDZ and m/z 346.2 for 1'-OH-MDZ-d_4 using Micromass Masslynx data analysis software. The metabolites were separated by Waters Alliance 2690 HPLC and an Agilent Zorbax XDB-C_8 5 µm column (2.1 mm i.d. x 50 mm) (Agilent Technologies, Palo Alto, CA). Gradient elution with 0.3 mL/min flow was used starting from 55% aqueous (0.1% acetic acid in water) and 45% methanol (0.1% acetic acid in methanol) to 60% methanol over 1.5 minutes, maintained for 0.5 min, followed by an increase to 90% methanol over 0.5 min, maintained for one minute and then returned to initial conditions. The percent remaining activity was plotted against the *trans*-ITZ concentrations and the IC_{50} values were determined by non-linear regression using GraphPad Prism, according to equation 1:

$$100\% \bullet \frac{v_i}{v} = \left(\frac{v_i}{v}\right)_{\min} \bullet 100\% + \frac{\left(\left(v_i/v\right)_{\max} - \left(v_i/v\right)_{\min} \bullet 100\%\right)}{\left(1+10^{(I-\log IC_{50})}\right)} \qquad (1)$$

in which $100\% \bullet \frac{v_i}{v}$ is the % activity remaining, $\left(\frac{v_i}{v}\right)_{\max} \bullet 100\%$ is the fitted % maximum activity remaining and $\left(\frac{v_i}{v}\right)_{\min} \bullet 100\%$ is the % minimum activity remaining. Terms v and v_i refer to the reaction velocity under control and inhibited conditions, I refers to the inhibitor concentrations and IC_{50} to the concentration of inhibitor that causes 50% inhibition of enzyme activity.

Determination of Ligand-Induced Binding Spectra: The binding mode and affinity of the *trans*-ITZ

DMD Fast Forward. Published on November 21, 2011 as DOI: 10.1124/dmd.111.042739
This article has not been copyedited and formatted. The final version may differ from this version.

isomers was determined by spectral titration with purified CYP3A4. The ligand-induced binding spectra (difference spectra) were recorded with Varian Cary 3E UV-Vis spectrophotometer. Matched cuvettes containing purified CYP3A4 (500 nM) in KPi buffer (pH 7.4) with 20 % glycerol at 22^{o}C were used. The *trans*-ITZ stereoisomers (0.005-3.96 µM) or M2 [1-(2,4-dichlorophenyl)-2-(1H-1,2,4-triazol-1-yl)ethanone] (1-127.2 µM) were added in 1 µl increments to the sample cuvette and the same volume of solvent was added to the reference cuvette. Ligand-induced difference spectra were recorded and, due to the tight binding of the ITZ stereoisomers with CYP3A4, the binding constant (K_s) values for ITZ stereoisomers were obtained by fitting the "Morrison" equation (Eq. 2) to the spectral titration data. The enzyme-inhibitor (EI) complex concentration was determined by Lambert-Beer law using the extinction coefficient determined from maximum absorbance detected when CYP3A4 protein was saturated as previously described (Kunze et al., 2006). In equation 2,

$$[EI] = \frac{[E]+[I]+K_s - \sqrt{([E]+[I]+K_s)^2 - 4[E][I]}}{2} \qquad (2)$$

K_s is the affinity constant of the ligand, [I] is the concentration of ligand, [E] is the concentration of enzyme, and [EI] is the concentration of the enzyme-ligand complex. For M2 the K_s was determined by fitting the Michaelis-Menten equation to the data.

Identification of Itraconazole Metabolites: *trans*-ITZ stereoisomers (1 µM) were incubated with CYP3A4 supersomes^{TM} (100 pmole) in 0.5 mL KPi buffer at 37^{o}C for 1 hr with and without NADPH. A conspectraltrol incubation with no supersomes was also included for each substrate. To determine whether the same metabolites were formed from *cis*-ITZs and from the 3'-OH-, keto- and N-desalkyl-ITZ these compounds were also incubated with CYP3A4 supersomes using similar conditions. The reactions were quenched with 1 mL of ethyl acetate. The extracted organic layer was dried under nitrogen gas in a water bath and the residues were reconstituted in 100 µL of ACN: H_2O (1:4). The metabolites were separated using a Shimadzu LC-10AD HPLC system equipped with an Agilent Zorbax

DMD Fast Forward. Published on November 21, 2011 as DOI: 10.1124/dmd.111.042739
This article has not been copyedited and formatted. The final version may differ from this version.

XDB-C_8 5 µm column (2.1 mm i.d. × 50 mm) by gradient elution (0.3 mL/min) from 90% aqueous (5 mM ammonium acetate) and 10% ACN to 40% ACN over 3 minutes, to 70% ACN over 3 minutes, then to 85% ACN over 3 minutes and to 95 % ACN over 1 minute followed by a 2 min hold before returning to initial conditions. The metabolites were detected with a Synapt High-Definition MS System, Quadrupole/Triwave™/Orthogonal acceleration time-of-flight tandem hybrid mass spectrometer (QToa-TOF) MS/IMS/MS (Waters, Milford, MA) operated on the positive ion electrospray mode monitoring ions m/z 100-1500 using cone voltage of 35 V with two modes: the low energy mode (collision energy 6 eV) for detection of the parent compounds and the high energy mode (ramped collision energy) for the fragmentation of the parent compounds. For the MS/MS analysis, the collision energy ramped from 11 to 30 eV for $[M+1]^+$ ion of m/z 466 and from 11 to 25 eV for $[M+1]^+$ ion of m/z 256. The resolving quadrupole (Q1) low mass resolution was 4.7 Da to collect fragmentation of all chlorine isotopes. The data was analyzed using Micromass Masslynx data analysis software.

The formation of M1 and M3, and reduction of M3 (m/z 466) to M1 (m/z 468) was monitored by Applied Biosystems API4000 MS/MS (AB Sciex, Foster City, CA) operated on the positive ion electrospray mode. The ions monitored were m/z 466.0 and m/z 468.0. The declustering potential was 60V and gas temperature was at 450^{o}C. The metabolites were separated as described above with a gradient from 80% aqueous (5 mM ammonium acetate) and 20% ACN to 50% ACN over 3 minutes, then to 60% ACN over 2 minutes and to 95% ACN over 0.1 minute followed by a 1.5 min hold at 95 % ACN before returning to initial conditions.

Characterization of catalytic rates of itraconazole metabolism: The catalytic rates (k_{cat}) for M2 formation were determined at saturating concentrations of the four *trans*-ITZs (500 nM) in incubations with CYP3A4 supersomes (1 pmol) in 0.5 mL KPi buffer at 37^{o}C for 1 minute after addition of NADPH (final concentration of 1 mM). The reaction mixtures were preincubated for 5 minutes at 37°C before NADPH addition. The k_{cat} was also determined based on results from incubations with reconstituted purified CYP3A4. CYP3A4 reconstitution was modified from the previous report (Shaw et al., 1997) to

DMD Fast Forward. Published on November 21, 2011 as DOI: 10.1124/dmd.111.042739
This article has not been copyedited and formatted. The final version may differ from this version.

include 5× CYP3A4 protein premix (0.5 µM P450 3A4, 1.0 µM NADPH-P450 reductase, 0.5 µM cytochrome b_5, 0.5 mg CHAPS/ml, 0.1 mg/ml liposomes [L-α-dilauroyl-*sn*-glycero-3-phosphocholine, L-α-dioleoyl-*sn*-glycero-3-phosphocholine, L-α-dilauroyl-*sn*-glycero-3-phosphoserine (1:1:1, w/w/w per ml)], 3.0 mM GSH, and 100 mM KPi buffer, pH 7.4) and a 5× buffer mix (100 mM KPi buffer, pH 7.4, 12 mM GSH, and 150 mM $MgCl_2$). For reconstitution, 60 µl of 5X CYP3A4 protein premix and equal volume of 5× buffer mix were mixed and left on ice for 10 min. *trans*-ITZ (1.67 µM) and KPi buffer were added to bring the volume to 0.294 mL. The mixture was preincubated at 37 ^oC for 3 min, followed by the addition of 6 µl of an NADPH solution (2 mM final concentration) to start the reaction and the reaction was allowed to proceed for 1 minute. The reactions were quenched with 1 mL ethyl acetate and internal standard (10 µl of 710 nM ITZ-d_5) was added. The organic layers were evaporated under a nitrogen stream, and the dry residue reconstituted in 100 µL of ACN/water (v/v, 1:4) and transferred to an LC/MS vial and analyzed using an Applied Biosystems API4000 MS/MS (AB SCIEX, Foster City, CA) as described above. The mass spectrometer was operated on the positive ion electrospray mode and MRM transitions of m/z 256.0 > 158.8 for M2 and m/z 712.32 > 399.23 for ITZ-d_5 were monitored. The declustering potential was 60 V, collision energy was 50 V, and gas temperature was at 450 ^oC. Gradient elution (0.3 mL/min) from 80% aqueous (5 mM ammonium acetate) and 20% ACN to 50% ACN over 3 minutes, to 60% ACN over 2 minutes and to 95% ACN over 0.1 minute followed by 1.5 min hold at 95 % ACN before returning to initial conditions was used. The standard curve was constructed based on extractions of M2 at concentrations from 0.039 to 30 nM. Data were analyzed using Analyst software (AB Sciex). The k_{cat} (pmol*min^{-1}pmol $P450^{-1}$) was calculated from amount of product formed divided by incubation time and amount of CYP3A4 in incubation.

Human Urine Sample Extraction: To establish the formation of M2 *in vivo* in humans**,** urine samples of six healthy volunteers before and after single oral *cis*-ITZ administration (400 mg) were analyzed. Urine samples were from previously conducted clinical itraconazole-midazolam drug-drug interaction study (Templeton et al., 2010). The University of Washington Institutional Review Board approved this

DMD Fast Forward. Published on November 21, 2011 as DOI: 10.1124/dmd.111.042739
This article has not been copyedited and formatted. The final version may differ from this version.

protocol. Six subjects were enrolled in the study (five males and one female). Urine samples were obtained for 24 h before and 12 and 12-24 h after itraconazole dosing (400 mg) and the volume of the urine was recorded. In addition, urine was collected for three additional 24 hour intervals, 24-48, 72-96 and 120-144 hours after the 400 mg itraconazole dose. The urine samples were stored at -20 °C until analysis. Urine samples (0.5 mL) were extracted with 1 mL of ethyl acetate and the residue was reconstituted in 100µL of acetonitrile: water (1:4). Samples were analyzed for M2 by LC-MS/MS using the Applied Biosystems API4000 MS as described above.

An additional metabolite was detected in the urine samples in the same MS/MS channel as M2. To identify this metabolite the same urine samples described above from two of the volunteers were reanalyzed. These urine samples (5 mL) were extracted with 25 mL of ethyl acetate and the residue was reconstituted in 100 µL of acetonitrile:water (1:4). The samples were analyzed using the Synapt High-Definition MS System, Quadrupole/Triwave™/Orthogonal acceleration time-of-flight tandem hybrid mass spectrometer (QToa-TOF) MS/IMS/MS as described above for incubation samples using the same chromatographic conditions. The parent mass was first determined via monitoring ions m/z 100-1000 using cone voltage of 35 V with two modes: a low energy mode (collision energy 6 eV) and a high energy mode (ramped collision energy from 10 to 40 eV). After identification of a metabolite with a mass of m/z 330, an MS/MS fragmentation pattern was collected for the metabolite. For the MS/MS analysis, the collision energy ramped from 10 to 40 eV for $[M+1]^+$ ion of m/z 330. All other detection and separation methods were as described above.

Surface Plasmon Resonance: The SPR experiments were performed as described previously for (2R,4S,2′R)-ITZ and CYP3A4 (Pearson et al., 2006). The sensor surface were pretreated as described previously and then normalized by standard Biacore protocols. Binding of the drug (2S,4S,2'S-ITZ 2, 4, 8 µM) to CYP3A4 in 3 % methanol in 100 mM KPi (pH 7.4) was monitored. For coupling of CYP3A4 to CM5 sensor surfaces, the surface was activated with a 5 min pulse of EDC/NHS (5 µL/min in HBS-EP buffer), followed by injection of the protein solution (400 nM in 10 mM sodium acetate

buffer, pH 5.5), and then deactivated by a 5 min pulse of ethanolamine HCl (pH 8.5, 5 μL/min). Protein injections were done for variable lengths of time to produce surfaces of variable protein densities, yielding responses that reached targeted 8 kRU. Blank control surfaces were activated and deactivated as the CYP3A4 immobilization process. SPR data were double-referenced and analyzed with Biacore T100 evaluation software (GE Healthcare). Dissociation phase data were fitted by one phase decay model to obtain a k_{off} rate constant using GraphPad Prism.

Results

To determine whether the four *trans*-ITZ stereoisomers bind to CYP3A4, their inhibitory potency was determined in human liver microsomes (HLMs) using midazolam as a probe substrate. The *trans*-ITZ concentration dependent inhibition of CYP3A4 is shown in Figure 1. The IC_{50} values for the four *trans*-ITZs were about 20 nM (Table 1) demonstrating that *trans*-ITZs are tight binding inhibitors of CYP3A4. To determine whether *trans*-ITZs also bind to CYP3A4 via triazole nitrogen coordinating to the heme iron, the ligand-induced difference spectra (binding spectra) of *trans*-ITZs were determined with purified CYP3A4 (Figure 2). All four *trans*-ITZ stereoisomers showed typical type II binding spectra with CYP3A4, characteristic of the triazole nitrogen coordinating to the heme and causing a high to low spin shift of the heme iron. The spectral dissociation constant, K_s, of the four *trans*-ITZ stereoisomers was determined from spectral titration (Figure 2) and the K_s values (obtained by fitting equation 2 to the data) ranged from 16 to 62 nM (Table 1), confirming the high affinity binding of all four *trans*-ITZ stereoisomers with CYP3A4.

Since *cis*-ITZ stereoisomers have previously been shown to undergo stereoselective metabolism by CYP3A4 despite their high affinity type II binding (Kunze et al., 2006), the metabolism of *trans*-ITZs by CYP3A4 was examined using CYP3A4 supersomes. The four *trans*-ITZs were not metabolized to the same metabolites as two of the *cis*-ITZs. No 3'-OH-ITZ, keto-ITZ or N-desalkyl-ITZ metabolites were found in *trans*-ITZ incubations, but considerable substrate depletion by recombinant CYP3A4 was observed. Since *trans*-ITZs were efficiently depleted by CYP3A4, the products from the incubations were analyzed using a Waters Synapt qTOF LC-MS/MS instrument to identify the metabolites formed. Two new metabolites, not observed in the control incubations (no NADPH and no enzyme), were detected from the incubations with *trans*-ITZs (Figure 3). The two metabolites had $[M+1]^+$ ions of m/z 468.261 (M1) and m/z 256.004 (M2) (Figure 3). The mass spectrum of M2 also showed a typical chlorine isotope pattern with an abundant isotope peak at m/z 258.0012 suggesting that this metabolite

DMD Fast Forward. Published on November 21, 2011 as DOI: 10.1124/dmd.111.042739
This article has not been copyedited and formatted. The final version may differ from this version.

retained the two Cl-atoms in ITZ. A similar isotope pattern is observed for ITZ as well. The MS/MS spectrum of M2 is shown in Figure 4. Based on the chloride isotope pattern and accurate mass (<5 ppm accuracy), M2 was tentatively identified as 1-(2,4-dichlorophenyl)-2-(1H-1,2,4-triazol-1-yl)ethanone (M2, Scheme 2). A reference material for M2 was commercially available and the MS/MS fragmentation pattern and retention time of the reference material was found to be identical to the enzymatically formed M2. Therefore M2 was confirmed as 1-(2,4-dichlorophenyl)-2-(1H-1,2,4-triazol-1-yl)ethanone (Scheme 2 and Figure 4A).

A tentative mechanism for the formation of M2 from ITZ by CYP3A4 was proposed (Scheme 2). Based on this proposed mechanism, the dioxolane ring is cleaved by CYP3A4 resulting in formation of M2 and a second metabolite with $[M+1]^+$ ion of m/z 466. However, the second metabolite M1 which was detected in the 1-hour incubations with CYP3A4 supersomes had an accurate mass that was 2 Da higher, $[M+1]^+$ of m/z 468.2610 (Figure 3). This mass difference suggested that M1 is a product from reduction of the aldehyde (M3a) or ketone (M3b) to an alcohol, resulting in the $[M+1]^+$ ion at m/z 468 (Scheme 2). It was hypothesized that M3a and/or M3b was reduced to M1 in the CYP3A4 supersomes in a non-P450 mediated manner. To test this hypothesis, the incubation time in supersomes was shortened and samples from seven different time points were analyzed by qTOF LC-MS/MS. Indeed, when *trans*-(2S,4S,2'S)-ITZ was incubated for 5 min with CYP3A4 supersomes, a metabolite with $[M+1]^+$ ion of m/z 466.2466 was detected (Figure 4B). Its formation was NADPH and enzyme dependent and the accurate mass of this metabolite was within 5 ppm of the calculated molecular ion of M3a and M3b (Scheme 2) consistent with the proposed mechanism for CYP3A4 mediated oxidative cleavage of the dioxolane ring. The MS/MS spectrum of this metabolite is shown in Figure 4C. As shown in the inset to Figure 4C, two peaks were detected in this m/z channel suggesting that both M3a and M3b were formed by CYP3A4.

To test whether the reduction of M3a and/or M3b to M1 was mediated by an endogenous reductase in

DMD Fast Forward. Published on November 21, 2011 as DOI: 10.1124/dmd.111.042739
This article has not been copyedited and formatted. The final version may differ from this version.

the CYP3A4 supersomes rather than CYP3A4, *trans*-(2S,4S,2'S)-ITZ was incubated with reconstituted purified CYP3A4 and CYP3A4 supersomes and the formation of the metabolites with $[M+1]^+$ m/z 466 (M3a and/or M3b) and $[M+1]^+$ m/z 468 (M1) was monitored. Formation of M3a/M3b was detected in both systems with similar abundance (2 min incubation time for reconstituted system; 3 min incubation time for supersomes) (Figure 5A and 5B). However, no formation of M1 was observed in incubations with purified reconstituted purified CYP3A4 (Figure 5A & C) whereas M1 was the dominant metabolite observed in incubations with CYP3A4 supersomes (Figure 5B & D). Based on this information, the mechanism shown in Scheme 2 for the CYP3A4 mediated dioxolane ring cleavage is proposed. Unfortunately no reference material for M3a or M3b is available and therefore it is not possible to confirm whether the observed metabolite has the structure of M3a and/or M3b and whether both of these metabolites are formed (Scheme 2). Methylene carbon 5 (Scheme 2) is sterically less hindered than is carbon 4, thus formation of M3a appears more likely. However, the MS/MS spectrum of the enzymatically formed product (Figure 4C) does not show any losses of CO (loss of m/z 28) or formaldehyde (loss of m/z 30), which would be expected from an aldehyde metabolite (M3a), suggesting that oxidation may occur at carbon 4. At present, it is not possible to differentiate between the two products.

To investigate whether the dioxolane ring scission is important for therapeutically administered ITZ (*cis*-ITZ), the four *cis*-ITZ stereoisomers and the CYP3A4 formed metabolites 3'-OH-ITZ, keto-ITZ and N-desalkyl-ITZ were incubated with CYP3A4 and the formation of M2 and M3a/M3b was monitored. Indeed, both M2 and M3a/M3b were detected in incubations with all four *cis*-ITZs, and M2 was detected in the incubations with 3'-OH-ITZ, keto-ITZ and N-desalkyl-ITZ (data not shown). These results demonstrate that dioxolane ring scission is a common metabolic pathway for all ITZ stereoisomers and their metabolites. The k_{cat} of M2 formation found for *trans*-ITZ was approximately 10 fold faster than the k_{cat} found for *cis*-ITZ. However, the rapid substrate depletion of *cis*-ITZs by CYP3A4 and the fact that M2 is formed from *cis*-ITZs as well as from the sequentially oxidized

DMD Fast Forward. Published on November 21, 2011 as DOI: 10.1124/dmd.111.042739
This article has not been copyedited and formatted. The final version may differ from this version.

metabolites makes it impossible to accurately characterize the kinetics of M2 formation from *cis*-ITZ.

The *trans*-ITZs do not undergo metabolism to 3'-OH-ITZ, keto-ITZ or N-desalkyl-ITZ. Therefore these ITZ stereoisomers offer a useful molecular probe for studying the interactions of ITZ with CYP3A4. It has previously been proposed that *cis*-ITZs have two binding orientations with CYP3A4 (Pearson et al., 2006), one of which allows the triazole ring to coordinate to the heme iron and another that brings the isobutyl side chain close to the heme for oxidation. Dissociation of *cis*-ITZ from CYP3A4 was proposed to be necessary for reorientation of ITZ within the CYP3A4 active site to allow metabolism to 3'-OH-ITZ. It was also found that the binding orientation in which the triazole ring coordinates to the heme iron has a slow dissociation rate that results in a "burst" in the metabolite formation kinetics from *cis*-ITZ. Since the dissociation rate for *cis*-ITZ is reportedly slow (0.0023 s^{-1}) and the dioxolane ring is adjacent to the triazole ring in ITZ, it is hypothesized that the dioxolane ring scission and CYP3A4-mediated oxidation of *trans*-ITZ occur without substrate dissociation from type II complex of the drug and CYP3A4. To test this hypothesis, the k_{cat} for M2 formation was measured for the four *trans*-ITZs at 500 nM substrate concentration. At this substrate concentration, product formation was linear with time and protein concentration. The k_{cat} values obtained for M2 formation from incubations of *trans*-ITZs with CYP3A4 supersomes and reconstituted CYP3A4 are summarized in Table 2. To compare the catalytic rate to the dissociation rate of *trans*-ITZs from CYP3A4, the k_{off} for *trans*-(2S,4S,2'S)-ITZ was measured using SPR. A k_{off} of 0.0072 s^{-1} was obtained by fitting the one phase decay model to the data (Figure 6). The fact that the off-rate is much slower than the measured k_{cat} in CYP3A4 supersomes suggests that the dioxolane ring scission occurs without dissociation and rebinding of *trans*-ITZ.

To determine whether the dioxolane ring scission occurs *in vivo* in humans, urine and plasma samples of six individuals following administration of 400 mg of ITZ orally were analyzed for presence of M2. M2 was found in all of the tested urine samples (Figure 7) but not in any of the plasma samples from the six subjects. The average amount of M2 found in the urine over 24 hours after 400 mg ITZ administration

to the six subjects was 1,114 ± 494 ng. As expected based on the long half-life of ITZ, M2 was detected in the urine 2, 4 and 7 days after ITZ administration and the average amount over 24 hour intervals was 429 ± 137 ng on day 2, 319 ± 192 ng on day 4 and 87 ± 31 ng on day 7. The total amount of M2 recovered in urine during these sampling periods suggests that it is a minor metabolite in urine. However, urine collection was incomplete and exact recovery of this metabolite cannot be determined. An additional unknown metabolite eluting at a retention time slightly before M2 was detected in the urine samples collected after ITZ administration but not in the samples collected prior to ITZ administration (Figure 7). To suggest a logical structure for this metabolite an accurate mass and MS/MS fragmentation pattern for this metabolite was collected. An MS/MS spectrum and the proposed ketal-carbinol structure (2-(2,4-dichlorophenyl)-2-(1H-1,2,4-triazol-1-yl)-1,3-dioxolane-4-methanol) is shown in Figure 7D. The mass accuracy for this structure was 2.4 ppm. The fragmentation was similar to that observed from M2, as expected

Since M2 was detected *in vivo* and it possesses a triazole ring in its structure, its inhibitory potency towards CYP3A4 was tested. The IC_{50}-value was found to be >15 µM (Figure 8 A), based on <50% inhibition at 15 µM M2 concentration. The affinity of M2 to CYP3A4 was further determined by spectral titration. A typical type II difference spectrum was obtained with purified CYP3A4 and the K_s value was 12.8 µM (Figure 8B). Based on the lack of detection of M2 in human plasma after ITZ administration and the high IC_{50} of M2, it is unlikely that this metabolite contributes to observed CYP3A4 inhibition *in vivo* after ITZ administration.

Discussion

Itraconazole is a strong inhibitor of the CYP3A4 mediated clearance of drugs in humans (Olkkola et al., 1996; Neuvonen et al., 1998) resulting in significant and persistent drug-drug interactions (DDIs). Based on recent studies, the magnitude and time-course of ITZ mediated DDIs result from inhibition of CYP3A4 by ITZ and its metabolites that are formed by CYP3A4 (Templeton et al., 2008; Templeton et al., 2010). In addition to inhibiting CYP3A4, *cis*-ITZs are also metabolized stereoselectively by CYP3A4 (Kunze et al., 2006). Two of the *cis*-ITZ isomers, (2R,4S,2'R)-ITZ and (2R,4S,2'S)-ITZ are metabolized by CYP3A4 to 3'-OH-, keto- and N-desalkyl-ITZ whereas the other two *cis*-ITZ stereoisomers do not undergo metabolism to these products (Kunze et al., 2006). Despite this observation, recombinant CYP3A4 depletes over 50% of the mixture of *cis*-ITZ isomers *in vitro* (Isoherranen et al., 2004), suggesting that all four *cis*-ITZ stereoisomers are substrates of CYP3A4. This study shows that dioxolane ring scission is another CYP3A4-mediated metabolic pathway for *cis*-ITZs and for the circulating *cis*-ITZ metabolites, 3'-OH-ITZ, keto-ITZ and N-desalkyl-ITZ.

In early studies in rats and dogs, dioxolane ring scission was proposed as a possible metabolic pathway of ITZ but the resulting products were not reported (Heykants et al., 1987), and no other metabolites of ITZ except 3'-OH-ITZ, keto-ITZ and N-desalkyl-ITZ have been quantified in humans. This study shows that the dioxolane ring scission is a clearance pathway of ITZ *in vivo*. This finding is of interest since the dioxolane ring is a common structural motif in many antifungal agents, including ketoconazole and terconazole and in related agricultural fungicides. In fact, the metabolite resulting from the dioxolane ring scission of ketoconazole (M+H m/z 255) was also observed in incubations of ketoconazole with CYP3A4 (data not shown). The cleavage of the dioxolane ring in propiconazole and formation of M2 has been previously reported (Chen et al., 2008) although the enzyme responsible for the reaction was not identified. The effects of M2 as a metabolite of propiconazole on cell viability was also evaluated in hepatic cells but no significant effects were detected. Based on these data it is likely

DMD Fast Forward. Published on November 21, 2011 as DOI: 10.1124/dmd.111.042739
This article has not been copyedited and formatted. The final version may differ from this version.

that dioxolane ring cleavage is a common metabolic pathway for the drugs in this class.

Even though M2 and M1 theoretically can be generated by acid catalyzed hydrolysis of the dioxolane ring (chiral center carbon, acetal), this mechanism is not likely in the *in vitro* incubations at pH 7.4 as no product was detected in the absence of NADPH. However, it is possible that after oral administration of ITZ the acidic conditions of the stomach could catalyze the cleavage. To test whether the hydrolysis occurs under acidic conditions, *cis*-ITZs (4 isomers), OH-, keto- and ND-ITZ were incubated in pH 2 at 37^{o}C for one hour, but no hydrolysis products or depletion of ITZ were observed (data not shown) suggesting acid catalyzed hydrolysis is unlikely.

Whether M2 has any biological activity is not currently known. Although M2 was a weak inhibitor of CYP3A4, it may have higher binding affinity to other drug metabolizing P450 enzymes or to P450 enzymes relevant for fungal cell survival. It is unlikely that the formation of M2 contributes to inhibition of CYP3A4 after ITZ administration based on the undetectable plasma concentrations and low inhibitory potency towards CYP3A4. However, if this metabolite is formed from other azole antifungals resulting in detectable plasma concentrations of it, further characterization of its inhibitory potency towards other CYPs is warranted due to the triazole group. The toxicological importance of the metabolites formed by dioxolane ring scission is not known. Both itraconazole and ketoconazole cause rare hepatotoxicity (Lewis et al., 1984; Wang et al., 2010) and it is possible that metabolites contribute to this adverse effect.

This study shows that *trans*-ITZs are as potent inhibitors of CYP3A4 as the *cis*-ITZs suggesting that the coordination of the triazole nitrogen to CYP3A4 heme and type II binding of ITZs in CYP3A4 active site are not sensitive to stereochemistry in the dioxolane ring or in the isobutyl side chain. The IC_{50} values for the four *trans*-ITZs were between 16 and 26 nM, which is similar to previously determined IC_{50} values of *cis*-ITZ isomers (4-15 nM) (Kunze et al., 2006). Thus, it seems surprising that the oxidation of the isobutyl side chain by CYP3A4 in *cis* and *trans*-ITZs is very stereoselective and that

the formation of M2 from *trans*-ITZs is significantly more efficient than from *cis*-ITZs. It is possible that the lack of 3'-OH-, keto- and N-desalkyl-ITZ formation from *trans*-ITZs is due to the preferential binding of the *trans*-ITZs with the triazole ring coordinating the heme, and the oxidation of the dioxolane ring occurs before the type II complex dissociates. Previous SPR studies (Pearson et al., 2006) showed that dissociation of the *cis*-ITZ must occur from type II binding orientation followed by rebinding in the catalytically accessible orientation (type I) to CYP3A4 in order for the metabolism to happen. For *trans*-ITZ the rapid catalysis of the dioxolane ring scission will not allow dissociation and rebinding of *trans*-ITZ in the alternative binding orientation with the isobutyl side chain close to the heme. This explanation was supported by the SPR data with *trans*-ITZ that showed that the dissociation rate of *trans*-ITZ from CYP3A4 (k_{off} = 0.0072 s^{-1}) is slower than the catalysis to M2 in CYP3A4 supersomes (k_{cat}=0.019 s^{-1}). These data also suggeststhat the heme iron is reduced with the type II ligand bound to the heme (low spin complex). This has been recently suggested for quinoline-4-carboxamide compounds with CYP3A4 (Pearson et al., 2011). Alternatively, the three dimensional structure of *trans*-ITZ may prevent the binding of these stereoiomers with the isobutyl side chain close to the heme due to unfavorable interactions between *trans*-ITZs and CYP3A4 active site residues in this orientation.

In summary, *trans*-ITZs are as potent inhibitors as *cis*-ITZs toward CYP3A4. Although the *trans*-ITZs are also substrates of CYP3A4, they are not metabolized to the corresponding *trans*- 3'-OH-, keto-, or N-desalkyl-ITZs. A metabolic pathway was identified in both *cis*- and *trans*-ITZ incubations with CYP3A4 and a new metabolite was formed from a type II binding compound that undergoes metabolism at a carbon close to the coordinating nitrogen. This metabolic pathway is likely to occur for other antifungals that contain a dioxolane ring in their structure, such as ketoconazole. This study increases our overall understanding of how the stereocenters of a substrate affect the metabolism and ligand interactions with CYP3A4, and provides unique insight into the structural determinants of ligand

metabolism by P450s.

Acknowledgments

The authors thank Peter Rademacher for the assistance in the high resolution mass spectrometry work, Kip Conner for his help in the SPR studies and Prof. William M. Atkins for helpful discussions during this work. The authors also wish to thank Dr. Connie Davis and Angela Hein for their efforts in the itraconazole clinical study.

Authorship Contributions:

Participated in Research Design: Peng, Kunze, Nelson, Isoherranen,

Conducted Experiments: Peng, Lutz

Contributed New Reagents or analytic tools: Shi, Liu

Performed Data analysis: Peng, Shi, Lutz, Kunze, Liu, Nelson, Isoherranen

Wrote or contributed to the writing of the manuscript: Peng, Lutz, Shi, Liu, Nelson, Isoherranen

REFERENCES

Chen P-J, Tanya M, and Stephen N (2008) Cytotoxic effects of propiconazole and its metabolites in mouse and human hepatoma cells and primary mouse hepatocytes. *Toxicol in Vitro* **22:**1476-1483.

Gillam EM, Baba T, Kim BR, Ohmori S, and Guengerich FP (1993) Expression of modified human cytochrome P450 3A4 in Escherichia coli and purification and reconstitution of the enzyme. *Arch Biochem Biophys* **305:**123-131.

Haria M, Bryson HM, and Goa KL (1996) Itraconazole. A reappraisal of its pharmacological properties and therapeutic use in the management of superficial fungal infections. *Drugs* **51:**585-620.

Heykants J, Michiels M, Meuldermans W, Monbaliu J, Lavrijsen K, Van Peer A, Levron J, Woestenborghs R, and Cauwenbergh G (1987) *The Pharmacokinetics of Itraconazole in Animals and Man: An Overview*. Prous Science Publishers, S.A.

Isoherranen N, Kunze KL, Allen KE, Nelson WL, and Thummel KE (2004) Role of itraconazole metabolites in CYP3A4 inhibition. *Drug Metab Dispos* **32:**1121-1131.

Kunze KL, Nelson WL, Kharasch ED, Thummel KE, and Isoherranen N (2006) Stereochemical aspects of itraconazole metabolism in vitro and in vivo. *Drug Metab Dispos* **34:**583-590.

Lewis JH, Zimmerman HJ, Benson GD, and Ishak KG (1984) Hepatic injury associated with ketoconazole therapy. Analysis of 33 cases. *Gastroenterology* **86:**503-513.

Neuvonen PJ, Kantola T, and Kivisto KT (1998) Simvastatin but not pravastatin is very susceptible to interaction with the CYP3A4 inhibitor itraconazole. *Clin Pharmacol Ther* **63:**332-341.

Olkkola KT, Ahonen J, and Neuvonen PJ (1996) The effects of the systemic antimycotics, itraconazole and fluconazole, on the pharmacokinetics and pharmacodynamics of intravenous and oral midazolam. *Anesth analgesia* **82:**511-516.

Omura T and Sato R (1964) The Carbon Monoxide-binding Pigment of Liver Microsomes II. Solubilization, Purification, Aand Properties. *J Biol Chem* **239:**2379-2385.

Pearson J, Dahal UP, Rock D, Peng CC, Schenk JO, Joswig-Jones C, and Jones JP (2011) The kinetic mechanism for cytochrome P450 metabolism of Type II binding compounds: Evidence supporting direct reduction. *Arch Biochem Biophys* **511:**69-79.

Pearson JT, Hill JJ, Swank J, Isoherranen N, Kunze KL, and Atkins WM (2006) Surface Plasmon Resonance Analysis of Antifungal Azoles Binding to CYP3A4 with Kinetic Resolution of Multiple Binding Orientations. *Biochemistry* **45:**6341-6353.

Shaw PM, Hosea NA, Thompson DV, Lenius JM, and Guengerich FP (1997) Reconstitution Premixes for Assays Using Purified Recombinant Human Cytochrome P450, NADPH-Cytochrome P450 Reductase, and Cytochromeb5. *Arch Biochem Biophys* **348:**107-115.

Shi W, Nacev BA, Bhat S, and Liu JO (2010) Impact of Absolute Stereochemistry on the Antiangiogenic and Antifungal Activities of Itraconazole. *ACS Med Chem Letters* **1** 155-159.

Templeton I, Peng C-C, Thummel KE, Davis C, Kunze KL, and Isoherranen N (2010) Accurate Prediction of Dose-Dependent CYP3A4 Inhibition by Itraconazole and Its Metabolites From In Vitro Inhibition Data. *Clin Pharmacol Ther* **88:**499-505.

Templeton IE, Thummel KE, Kharasch ED, Kunze KL, Hoffer C, Nelson WL, and Isoherranen N (2008) Contribution of Itraconazole Metabolites to Inhibition of CYP3A4 In Vivo. *Clin Pharmacol Ther* **83:**77-85.

Vanden Bossche H, Marichal P, Gorrens J, Coene MC, Willemsens G, Bellens D, Roels I, Moereels H, and Janssen PA (1989) Biochemical approaches to selective antifungal activity. Focus on azole antifungals. *Mycoses* **32 Suppl 1:**35-52.

Wang JL, Chang CH, Young-Xu Y, and Chan KA (2010) Systematic review and meta-analysis of the tolerability and hepatotoxicity of antifungals in empirical and definitive therapy for invasive fungal infection. *Antimicrob Agents Chemother* **54:**2409-2419.

Footnotes

This work was supported in part by the National Institutes of Health National Institute of General Medical Sciences [Grant P01-GM32165] (NI, KLK and WLN) and National Cancer Institute [Grant CA122814] (JOL).

DMD Fast Forward. Published on November 21, 2011 as DOI: 10.1124/dmd.111.042739
This article has not been copyedited and formatted. The final version may differ from this version.

Legends to Schemes

Scheme 1. The structure of itraconazole with three stereocenters (2, 4, and 2') indicated with an asterisks on the upper left. One example of cis- and trans-ITZ is shown on the upper right. The three metabolites of cis-ITZ are shown below the ITZ structure.

Scheme 2. Proposed mechanism for the formation of the new ITZ metabolite.

DMD Fast Forward. Published on November 21, 2011 as DOI: 10.1124/dmd.111.042739
This article has not been copyedited and formatted. The final version may differ from this version.

Figure legends

Figure 1. Inhibition of CYP3A4 by *trans*-ITZ stereoisomers. IC_{50} inhibition of CYP3A4 by trans-ITZs in human liver microsomes using midazolam as the probe substrate. IC_{50} was determined by fitting equation 1 to the data.

Figure 2. Binding of *trans*-ITZ in CYP3A4 active site. UV-Vis difference spectra of CYP3A4 with *trans*-ITZs. The spectral titration curves are shown in the insets. The K_s value for each *trans*-ITZs was determined from fitting to the quadratic equation (Morrison, equation 2) to the titration data.

Figure 3. Identification of metabolites generated from trans-ITZs by CYP3A4. A representative chromatogram of an incubation of *cis*- and *trans*-ITZs with CYP3A4. When incubated in the presence of CYP3A4 supersomes^{TM}, both *cis*- and *trans*-ITZ form the new ITZ metabolites (M1 and M2). The new metabolites were not found in the absence of CYP3A4 or NADPH control samples as shown in the control traces. The MS data were collected by full scan using Synapt Q-TOF for high accuracy MS. Ions monitored are m/z 100-1500 in low energy mode, the cone voltage was 35 V and the collision energy was 6 eV as described in Materials and Methods.

Figure 4. Characterization of M2 and M3 as metabolites of itraconazole. The MS/MS spectrum of M2 (parent $[M+1]^+$ m/z 256) formed from ITZ in incubation with CYP3A4 is shown in panel A. The MS/MS spectrum was identical to that obtained from the reference standard of M2. Panel B shows the molecular ion of M3 and panel C shows the MS/MS spectrum of M3 (parent ion $[M+1]^+$ m/z 466). The insets show the selected ion chromatograms for the parent ion. The spectra were collected using Synapt Q-TOF LC-MS as described in materials and methods.

Figure 5. Characterization of the formation of M1 and M3 by CYP3A4 microsomes and reconstituted CYP3A4. Selected ion chromatograms of m/z 466 and m/z 468 recorded with Applied

Biosystems API4000 MS/MS as described in Materials and Methods. *trans*-(2S,4S,2'S)-ITZ was incubated with purified CYP3A4 reconstituted with P450 reductase (A and C) and CYP3A4 supersomes (B and D) and the formation of M1 and M3 was followed at m/z 468 and m/z 466. The metabolite M3, m/z 466, was found in both enzyme systems; however, reduction to M1, m/z 468, only occurred in the Supersome incubation.

Figure 6. Determination of the dissociation rate for (2S,4S,2'S)-ITZ from CYP3A4 using surface plasmon resonance (SPR). The dissociation rate (k_{off}) of (2S,4S,2'S)-ITZ was determined by one phase decay model and the k_{off} was found to be $0.0072 \pm 0.0006 s^{-1}$. Only the dissociation phase of the SPR run is shown.

Figure 7. Detection of M2 in urine samples from healthy volunteers after administration of 400 mg itraconazole and identification of an additional metabolite of ITZ in urine. Samples were analyzed as described in materials and methods. M2 was detected by MS/MS using ion transition of m/z 256>158. Panel A shows a representative chromatogram of a urine sample from a study subject before ITZ administration; panel B shows a chromatogram of M2 standard extracted from blank urine and panel C shows a representative chromatogram of a urine sample after administration of 400 mg ITZ orally. In panel C the peak at 2.75 min is M2 and a second unknown metabolite was detected at an earlier elution time 2.45. To identify this metabolite the urine samples were reanalyzed as described in materials and methods and accurate mass as well as the fragmentation pattern of this metabolite was obtained (panel D). The MS/MS spectrum of this additional metabolite sows the fragmentation to the two monitored ions m/z 256 and m/z 159 as well as the chloride isotope pattern characteristic of two chloride ions present in the metabolite and fragments.

Figure 8. Determination of the inhibitory potency of M2 towards CYP3A4. A) Inhibition of CYP3A4 mediated midazolam hydroxylation in human liver microsomes by M2. The percent remaining

activity versus M2 concentrations is shown. The IC_{50} of M2 toward CYP3A4 was determined to be >15 μM. B) Binding of M2 to purified CYP3A4 shows a type II binding spectrum demonstrating triazole coordination to the heme. The K_s of M2 was determined by spectral titration as described in materials and methods (K_s = 12.8 ± 1.1 μM) and the increased absorbance as a function of M2 concentration is shown in the inset. The Michaelis-Menten equation was fitted to the data to obtain the K_s value.

DMD Fast Forward. Published on November 21, 2011 as DOI: 10.1124/dmd.111.042739
This article has not been copyedited and formatted. The final version may differ from this version.

Table 1. Inhibitory potency (IC_{50}) of *trans*-ITZ stereoisomers toward CYP3A4 determined in human liver microsomes (IC_{50}) and spectroscopic dissociation constants (K_s) determined using purified CYP3A4.

trans-	(2R,4R,2'R)-ITZ	(2R,4R,2'S)-ITZ	(2S,4S,2'S)-ITZ	(2S,4S,2'R)-ITZ
IC_{50} (nM)	26 ± 1	20 ± 1	16 ± 1	17 ± 1
K_s (nM)	23.8 ± 11.2	61.7 ± 17.4	16.1 ± 12.2	31.9 ± 4.1

DMD Fast Forward. Published on November 21, 2011 as DOI: 10.1124/dmd.111.042739
This article has not been copyedited and formatted. The final version may differ from this version.

Table 2. The catalytic rate constants (k_{cat}-values) for formation of M2 from trans-ITZ stereoisomers in incubations with reconstituted CYP3A4 and with CYP3A4 supersomes. Catalytic rates could not be measured for *cis*-ITZ stereoisomers due to high substrate depletion and formation of M2 from multiple substrates simultaneously.

trans-	(2R,4R,2'R)-ITZ	(2R,4R,2'S)-ITZ	(2S,4S,2'S)-ITZ	(2S,4S,2'R)-ITZ
k_{cat} (s^{-1}) reconstituted CYP3A4	0.0032 ± 0.0005	0.0038 ± 0.0001	0.0041 ± 0.0007	0.0042 ± 0.0004
k_{cat} (s^{-1}) CYP3A4 supersomes	0.0159 ± 0.003	0.0214 ± 0.004	0.0183 ± 0.003	0.0198 ± 0.001

scheme 1

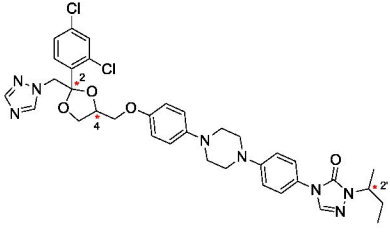

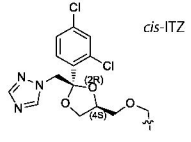

cis-ITZ

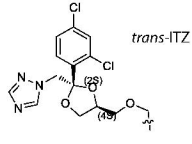

trans-ITZ

OH-ITZ

keto-ITZ

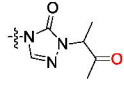

N-desalkyl-ITZ

Scheme 2

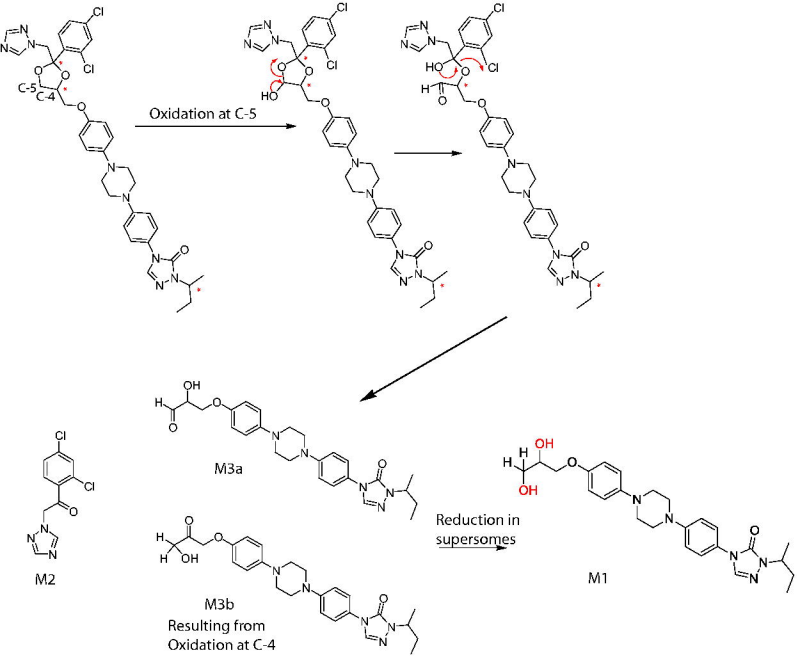
C-5
C-4
Oxidation at C-5
M3a
M2
M3b
Resulting from
Oxidation at C-4
Reduction in
supersomes
M1

Figure 1

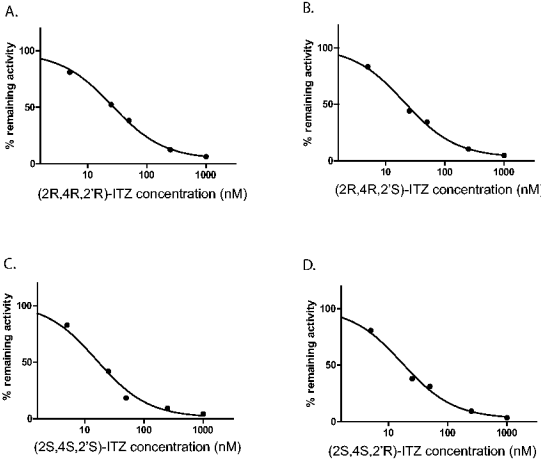
A.
% remaining activity
100
50
0
10
100
1000
(2R,4R,2'R)-ITZ concentration (nM)
B.
% remaining activity
100
50
0
10
100
1000
(2R,4R,2'S)-ITZ concentration (nM)
C.
% remaining activity
100
50
0
10
100
1000
(2S,4S,2'S)-ITZ concentration (nM)
D.
% remaining activity
100
50
0
10
100
1000
(2S,4S,2'R)-ITZ concentration (nM)

Figure 2

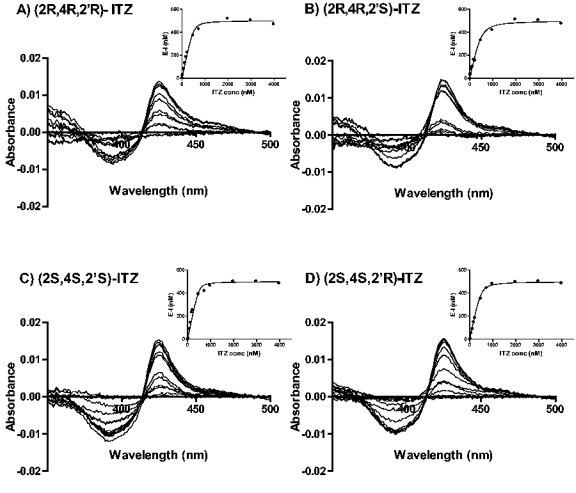
A) (2R,4R,2'R)- ITZ
B) (2R,4R,2'S)-ITZ
C) (2S,4S,2'S)-ITZ
D) (2S,4S,2'R)-ITZ
Absorbance
Wavelength (nm)
ITZ conc (nM)

Figure 3

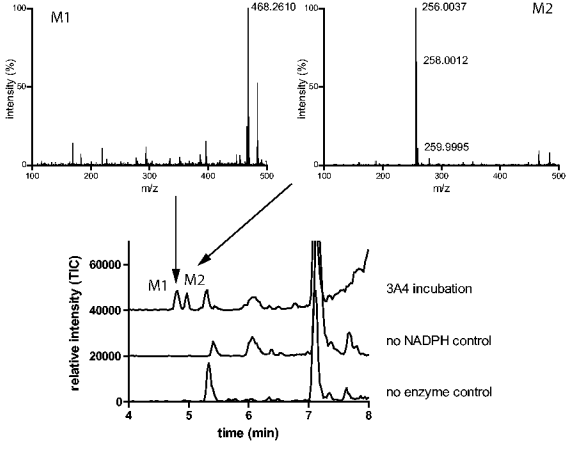
M1
468.2610
intensity (%)
m/z
M2
256.0037
258.0012
259.9995
relative intensity (TIC)
time (min)
3A4 incubation
no NADPH control
no enzyme control

Figure 4

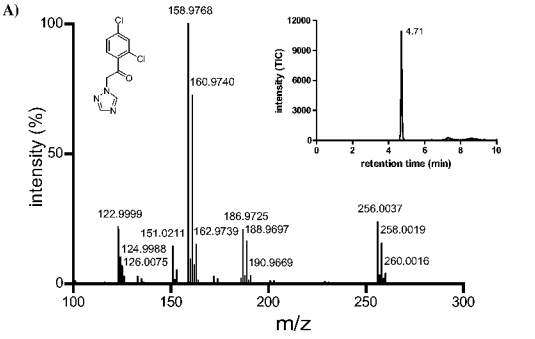
A)
intensity (%)
m/z
158.9768
160.9740
122.9999
151.0211
124.9988
126.0075
162.9739
186.9725
188.9697
190.9669
256.0037
258.0019
260.0016
intensity (TIC)
retention time (min)
4.71

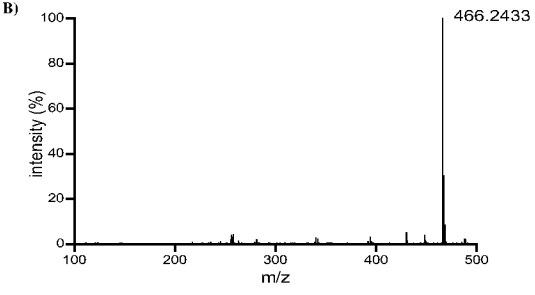
B)
intensity (%)
m/z
466.2433

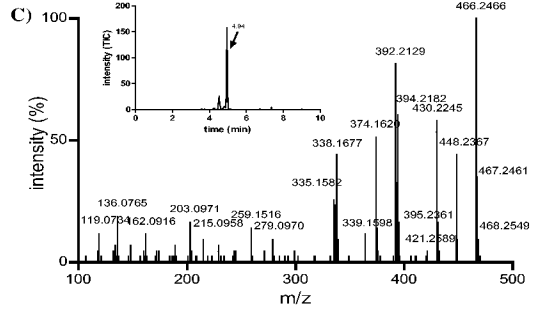
C)
intensity (%)
m/z
intensity (TIC)
time (min)
4.94
466.2466
392.2129
394.2182
430.2245
374.1620
338.1677
448.2367
467.2461
335.1582
136.0765
119.0784
162.0916
203.0971
215.0958
259.1516
279.0970
339.1598
395.2361
421.2589
468.2549

Figure 5

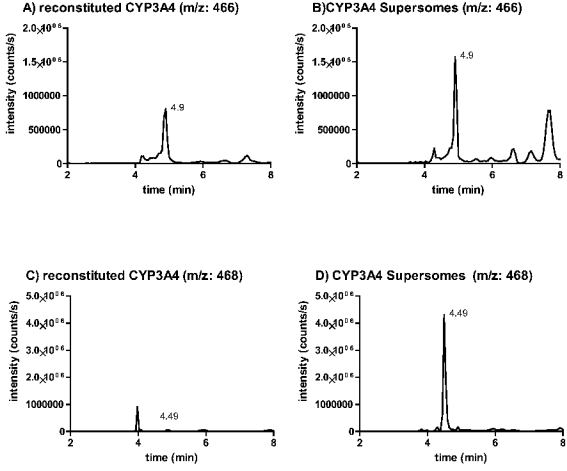
A) reconstituted CYP3A4 (m/z: 466)
B)CYP3A4 Supersomes (m/z: 466)
C) reconstituted CYP3A4 (m/z: 468)
D) CYP3A4 Supersomes (m/z: 468)
intensity (counts/s)
time (min)
4.9
4.49

Figure 6

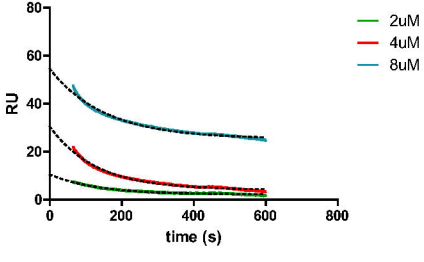

Figure 7

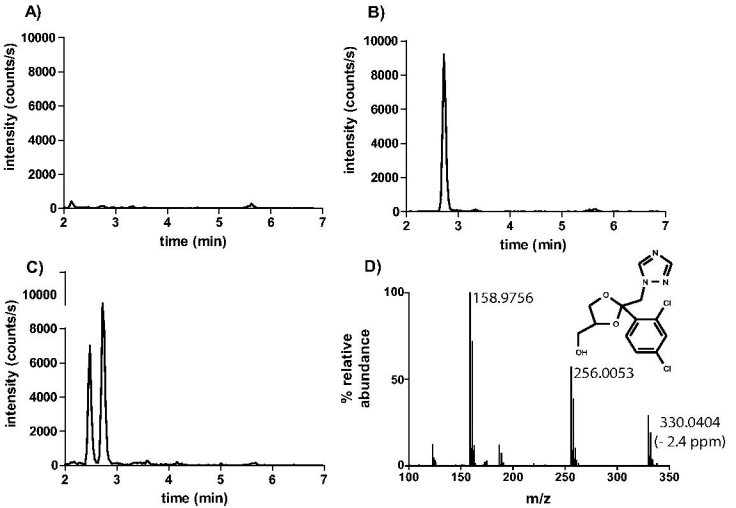
A)
intensity (counts/s)
time (min)
B)
intensity (counts/s)
time (min)
C)
intensity (counts/s)
time (min)
D)
% relative abundance
158.9756
256.0053
330.0404
(- 2.4 ppm)
m/z

Figure 8

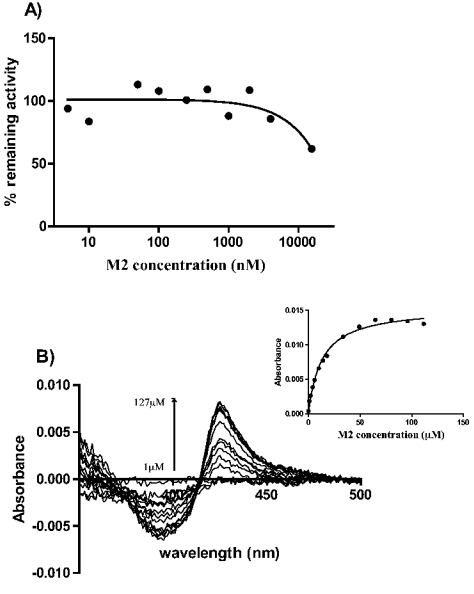
A)
150
100
50
0
% remaining activity
10
100
1000
10000
M2 concentration (nM)
B)
0.010
0.005
0.000
-0.005
-0.010
Absorbance
127μM
1μM
400
450
500
wavelength (nm)
0.015
0.010
0.005
0.000
Absorbance
0
50
100
150
M2 concentration (μM)